Magnetovolume effects and spin fluctuations in $Mn_{3+x}Rh_{1-x}$ alloys

2003 J. Phys.: Condens. Matter 15 4589

(http://iopscience.iop.org/0953-8984/15/26/309)

INSTITUTE OF PHYSICS PUBLISHING JOURNAL OF PHYSICS: CONDENSED MATTER

J. Phys.: Condens. Matter **15** (2003) 4589–4604 PII: S0953-8984(03)60602-8

Magnetovolume effects and spin fluctuations in $Mn_{3+x}Rh_{1-x}$ alloys

R Y Umetsu[1,4], K Fukamichi[1], Y Fujinaga[2] and A Sakuma[3,5]

[1] Department of Materials Science, Graduate School of Engineering, Tohoku University, Aoba-yama 02, Sendai 980-8579, Japan
[2] Institute for Materials Research, Tohoku University, Katahira, Sendai 980-8577, Japan
[3] Advanced Electronics Research Laboratory, Hitachi Metals, Ltd, Mikajiri, Kumagaya, Saitama 360-0843, Japan

E-mail: rie@maglab.material.tohoku.ac.jp

Received 6 March 2003
Published 20 June 2003
Online at stacks.iop.org/JPhysCM/15/4589

Abstract

The electrical resistivity, thermal properties, pressure effect on the Néel temperature and compressibility of $Mn_{3+x}Rh_{1-x}$ ($x = 0.0$, 0.12, 0.20 and 0.32) alloys have been investigated in order to discuss the magnetovolume effects in both ordered and disordered states. The electronic specific heat coefficient γ^{exp} of the Mn_3Rh ordered alloy is slightly smaller than that of the disordered one, qualitatively consistent with the theoretical calculations. A negative magnetovolume effect is observed below the Néel temperature T_N in both the ordered and disordered alloys. Furthermore, the magnetic contribution to the thermal expansion is significant even in the paramagnetic region. That is, the thermal expansion coefficient α in the paramagnetic region shows a large value of about 30×10^{-6} K^{-1}, because of a significant contribution from spin fluctuations. For the Mn_3Rh ordered alloy, the pressure shift of the Néel temperature, dT_N/dP, is estimated to be about 7.0 K GPa^{-1}. The temperature dependence of α exhibits a pronounced positive peak at T_N in accordance with the positive pressure dependence of T_N. A large compressibility of 1.4×10^{-2} GPa^{-1} has been obtained from the change in the lattice constant under pressure.

1. Introduction

Pure γ-Mn is stable between 1373 and 1411 K [1], and this phase cannot be retained by quenching. By adding a small amount of elements such as Cu [2], Fe [3], Ni [4] and Ge [5], γ-phase Mn alloys are stabilized by quenching from high temperatures, and this phase is

[4] Author to whom any correspondence should be addressed.
[5] Present address: Department of Applied Physics, Graduate School of Engineering, Tohoku University, Aoba-yama 08, Sendai 980-8579, Japan.

0953-8984/03/264589+16$30.00

antiferromagnetic with a high Néel temperature of several hundred kelvin. A large amount of additives such as Rh, Pt and Ir also stabilizes an ordered γ-phase having a $AuCu_3$-type crystal structure [6]. Mn_3Rh, Mn_3Pt and Mn_3Ir ordered phases have a triangular-type spin structure, in which the Mn moments lie in the (111) plane [7–9] and their Néel temperature is higher than that of their counterparts in the disordered phase [10–13]. It is well known that the magnetic properties of Mn alloy systems are very sensitive to the Mn–Mn distance [14]. For example, the concentration dependence of the order–order transition temperature and the pressure effect on the Néel temperature of the Mn_3Pt ordered alloy have been explained by the relation between the strength of exchange interaction and the Mn–Mn distance within the framework of localized electron models [15, 16]. However, recently, it has been pointed out that the magnetic properties of the Mn_3Pt ordered alloy should be interpreted in terms of the band model [17]. We have investigated magnetic properties of the γ-phase Mn–Rh alloy system in the ordered and disordered states [12, 18, 19], and pointed out that the Néel temperature, or the strength of the exchange interaction, should be connected with the number of 3d electrons in the Mn site [20].

It has been reported that α-Mn exhibits a notably low bulk modulus [21]. For the theoretical results [22, 23], the bulk modulus of the transition metals exhibits a systematic behaviour with increasing atomic number and the results of 4d transition metal series are consistent with the experimental results. This behaviour can be understood qualitatively by the increase of d electrons with the atomic number. However, the situation is less systematic for 3d transition metal series. The observed bulk moduli of five magnetic elements, Cr, Mn, Fe, Co and Ni, are lower than the calculated ones; in particular, the value of Mn is most deviant [22, 23]. It has been pointed out that there is a close relationship between the bulk modulus and the magnitude of magnetic moment for 3d transition metals and alloys [24]. The low bulk modulus of α-Mn would be attributed to the presence of the magnetic moment of the Mn atom [14]. On the other hand, so far as we know, there has been no report on the bulk modulus of γ-phase Mn alloys.

For practical applications, γ-phase Mn-based alloys such as Mn–Ir [25–27] and Mn–Rh [28, 29] disordered alloys are intensively investigated for spin-valve devices comprised by several kinds of magnetic layer. Thermal strains induced by the difference between the thermal expansions of the multilayers and also the magnetovolume effects are closely correlated to the durability and stability of the spin-valves because atomic diffusions are accelerated by electromigration and stress migration. In addition, the exchange-biasing characteristics and the blocking temperature are closely correlated with the spin structures and the magnitude of the Néel temperature [30–32]. It has been reported from the experimental and theoretical investigations that Mn–Ir [13, 33] and Mn–Rh [19, 34] disordered alloys have multiple-Q spin density waves (MQSDWs) and the spin structure changes with temperature and/or composition. Therefore, in order to design spin-valve devices with excellent properties, investigations of fundamental physical properties are highly desired.

In the present paper, the electrical resistivity, low-temperature specific heat and thermal expansion of the $Mn_{3+x}Rh_{1-x}$ ($x = 0.0$, 0.12, 0.20 and 0.32) ordered and disordered alloys are discussed. The theoretical energy calculations for the magnetic structure are carried out in order to discuss the magnetic stability of the Mn_3Rh ordered and disordered alloys. Finally, the effect of pressure on the Néel temperature and compressibility of the Mn_3Rh ordered alloy are obtained from the electrical resistivity data in order to discuss the correlation between the thermal expansion characteristics and the pressure dependence of the Néel temperature.

2. Experiment and calculation

The starting materials were 99.98 % pure electrolytic Mn flakes and 99.95 % pure Rh powders. Before alloying, surface oxidation of the Mn flakes was removed by etching with a very

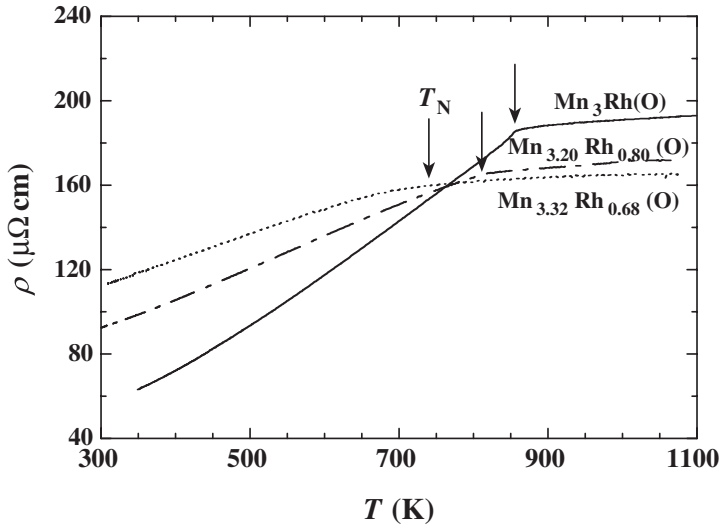

Figure 1. Temperature dependence of electrical resistivity ρ of the Mn_3Rh, $Mn_{3.20}Rh_{0.80}$ and $Mn_{3.32}Rh_{0.68}$ ordered (O) alloys. The arrows indicate the Néel temperature T_N.

dilute nitric acid, and arc-melted in order to release gas in the Mn flakes. The Rh powders were also arc-melted in order to make the Rh ingots. The specimens were prepared by arc-melting in an argon gas atmosphere, and turned over and remelted four times. In order to homogenize the specimens were annealed for ten days at 873 K in an evacuated quartz tube. The specimens were annealed at 1373 K and subsequently quenched rapidly into ice water in order to make the disordered state. To confirm the quality of the specimens, x-ray powder diffraction measurements were carried out at room temperature. The alloy compositions were determined by energy dispersive x-ray spectroscopy (EDXS).

The temperature dependences of electrical resistivity and specific heat were measured by a four-probe method and a relaxation method, respectively. The thermal expansion measurements were made with a differential transformer-type dilatometer. The effect of pressure on the Néel temperature was investigated by the electrical resistivity measurement under various pressures with a cubic-type multianvil press. The room temperature x-ray powder diffraction by an energy-dispersive mode at a fixed diffraction angle was made under pressure applying up to about 6.0 GPa by using the same cubic-type multianvil press.

The magnetic structures were calculated by the tight-binding (TB) linear muffin-tin orbital (LMTO) method based on the local spin density (LSD) functional approximation. Non-collinear magnetic structures were treated through the local rotation of the spin quantization axis on each site. In both the disordered and paramagnetic states, the coherent potential approximation (CPA) was used for each sub-lattice within the local frame of the spin axis. Detailed calculation methods and a brief explanation of the theoretical methodology have been described elsewhere [34, 35].

3. Results and discussion

Figure 1 shows the temperature dependence of electrical resistivity ρ of Mn_3Rh, $Mn_{3.20}Rh_{0.80}$ and $Mn_{3.32}Rh_{0.68}$ ordered (O) alloys. In the figure, the arrows indicate the Néel temperature T_N determined from our previous magnetic data [18] which coincide with the reported neutron

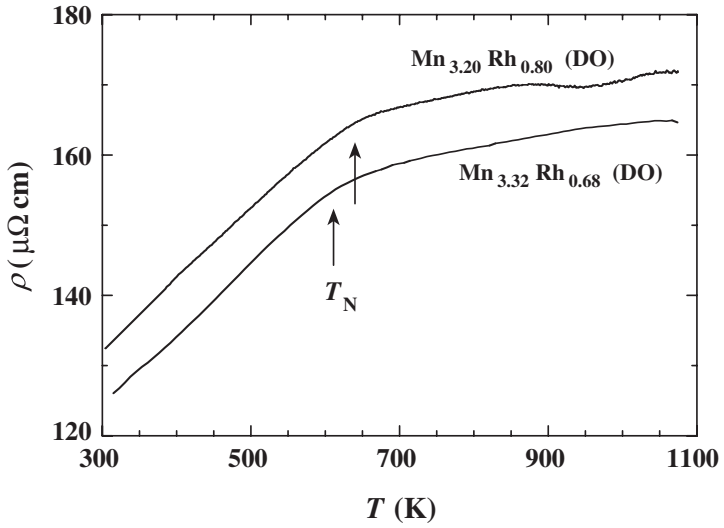

Figure 2. Temperature dependence of electrical resistivity ρ of the $Mn_{3.20}Rh_{0.80}$ and $Mn_{3.32}Rh_{0.68}$ disordered (DO) alloys. The arrows indicate the Néel temperature T_N.

diffraction data [8]. Antiferromagnetic materials exhibit two types of electrical resistivity curve, depending on band structures. One is a gap type, showing a hump below T_N in the electrical resistivity curve; the other is a gapless type, which exhibits a steeper decrease below T_N [36, 37]. The present electrical resistivity curves tell us that these ordered alloys fall into the latter case. On the other hand, equi-atomic MnPt [38] and MnPd [39] $L1_0$-type alloys which are also used for pinning layers of spin-valves are classified into the former case. The anomaly at T_N in the electrical resistivity curves for the stoichiometric composition Mn_3Rh is clearest, becoming weaker with decreasing Rh concentration.

The temperature dependences of electrical resistivity ρ of the $Mn_{3.20}Rh_{0.80}$ and $Mn_{3.32}Rh_{0.68}$ disordered (DO) alloys are shown in figure 2. The Néel temperature T_N indicated by the arrows in the figure is also determined from our previous magnetic data [18] and T_N of the disordered alloys is lower than that of the ordered alloys. The anomaly at T_N is not so clear for these disordered alloys in analogy with their magnetic data [12]. An additional anomaly observed around 930 K for the $Mn_{3.20}Rh_{0.80}$ is correlated to the atomic ordering. It is difficult to confirm T_N for the Mn_3Rh disordered alloy because T_N is very close to the atomic ordering temperature. The atomic ordering temperature of the $Mn_{3.32}Rh_{0.68}$ would become above 1100 K, because no distinct anomaly in the curve is confirmed as seen from the figure.

Shown in figure 3 is the temperature dependence of the low-temperature specific heat C plotted in the form of C/T–T^2 for the ordered (O) and disordered (DO) alloys. The closed and open circles indicate the specific heat C of the Mn_3Rh ordered and disordered alloys, respectively. The closed and open triangles indicate C of the $Mn_{3.20}Rh_{0.80}$ ordered (O) and disordered (DO) alloys, respectively. In the C/T–T^2 plots, the intercept gives the electronic specific heat coefficient γ^{exp} and the slope is proportional to $1/\Theta_D^3$. From the figure, the values of γ^{exp} for the Mn_3Rh ordered (O) and disordered (DO) alloys are deduced to be about 4.0 and 4.6 mJ mol^{-1} K^{-2}, respectively, and those of the $Mn_{3.20}Rh_{0.80}$ ordered (O) and disordered (DO) alloys to be about 6.8 and 7.1 mJ mol^{-1} K^{-2}, respectively. The Debye temperature Θ_D scarcely depends on the concentration being about 310 K. The electronic structures of the stoichiometric Mn_3Rh ordered and disordered alloys have been calculated [34]. The magnetic

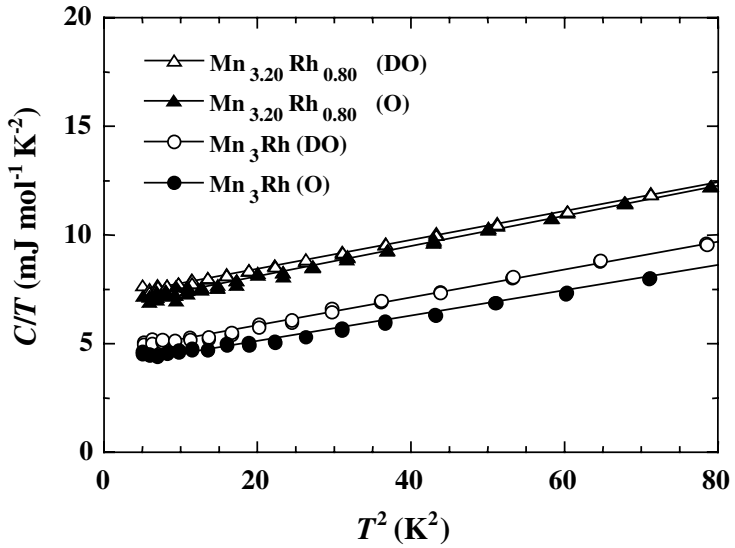

Figure 3. Temperature dependence of the specific heat C in the form of C/T–T^2. The closed and open circles indicate C of the Mn_3Rh ordered (O) and the disordered (DO) alloys, respectively. The closed and open triangles indicate C of the $Mn_{3.20}Rh_{0.80}$ ordered (O) and the disordered (DO) alloys, respectively.

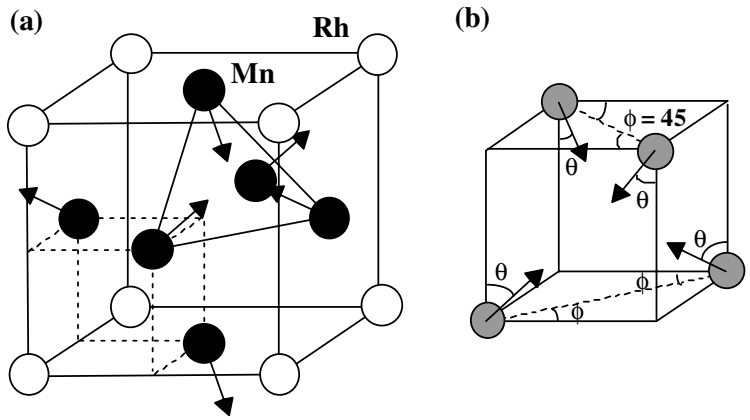

Figure 4. (a) Magnetic structure of the T1 for the Mn_3Rh ordered alloy [7, 8]. One cubic cell indicates one-eighth of the unit cell having the fcc lattice. (b) MQSDW structure of the disordered alloy [34]. The $1Q$, $2Q$ and $3Q$ SDW structures are realized by putting $\theta = 0°, 90°$ and $54.7°$, respectively.

structures in the ordered and disordered alloys are shown in figures 4(a) and (b), respectively. Figure 4(a) shows the T1 (triangular-type) structure [7, 8], in which the Mn moments lie in the (111) plane. One cubic cell of figure 4(b) indicates one-eighth of the chemical unit cell having an fcc crystal structure given by the dotted cell in figure 4(a) and the MQSDW structures can be drawn as a function of θ and also ϕ. For γ-phase Mn disordered alloys, such as Mn–Ni [40] and Mn–Ga [41], the $1Q$, $2Q$ and $3Q$ spin density wave (SDW) structures are observed by changing temperature and/or composition. In the figure, setting $\phi = 45$, these three structures

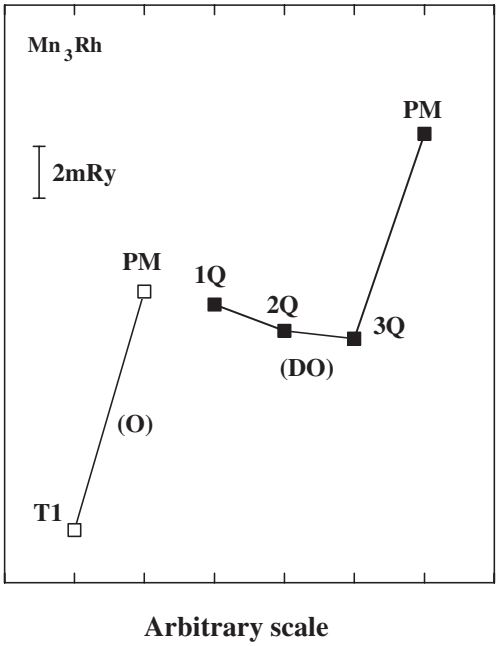

Figure 5. Relative difference between the total energy of the Mn_3Rh ordered (O) and disordered (DO) alloys with each magnetic structure.

are realized by putting $\theta = 0°, 90°$ and 54.7°, respectively. That is, in $1Q$ and $2Q$ SDW structures, the magnetic moment points parallel and perpendicular to the c-axis, respectively, and the $3Q$ SDW structure is intact to figure 4(b). The detailed calculated results, the electronic structures and the effective exchange constant, for the Mn_3Rh ordered and disordered alloys, have been discussed elsewhere [34]. In figure 5, we show the relative difference in the total energy calculated by using the CPA with the TB-LMTO method for the Mn_3Rh ordered (O) and disordered (DO) alloys with each magnetic structure to give a visual representation. For convenience, the abscissa is divided into the equidistance for each magnetic structure. The $3Q$ SDW structure is found to have the lowest energy in the disordered state. These calculated results are in accord with the phase diagram of the Mn–Rh disordered alloy system given from the experimental data [19]. Furthermore, the calculated electronic structures predict that the dip is formed around the Fermi level E_F, and the dip of the ordered alloy is more distinct than that of the disordered alloy. The total density of states (DOS) at E_F of the Mn_3Rh ordered and disordered alloys can be estimated to be about 9 and 13 (1/Ryd atom spin), respectively, and the γ^{cal}-value is deduced to be about 1.6 and 2.2 mJ mol^{-1} K^{-2} from the following relation, neglecting the electron–phonon coupling term:

$$\gamma^{cal} = \tfrac{1}{3}\pi^2 k_B^2 N(E_F), \tag{1}$$

where k_B and $N(E_F)$ are the Boltzmann constant and the total DOS at E_F, respectively. The calculated total energy (ΔE in mRyd/atom), the magnetic moment (M in μ_B), the effective exchange constant (J_0 in millielectronvolts), the Néel temperature (T_N^{cal} in kelvin) estimated from $2J_0/3k_B$, the Néel temperature (T_N^{exp} in kelvin) given by the experiments and the electronic specific heat coefficient obtained by the calculation (γ^{cal} in mJ mol^{-1} K^{-2}) and the experiment (γ^{exp} in mJ mol^{-1} K^{-2}) for the Mn_3Rh ordered (O) and disordered (DO) alloys are listed in table 1. According to the generalized molecular field theory, the value of T_N can

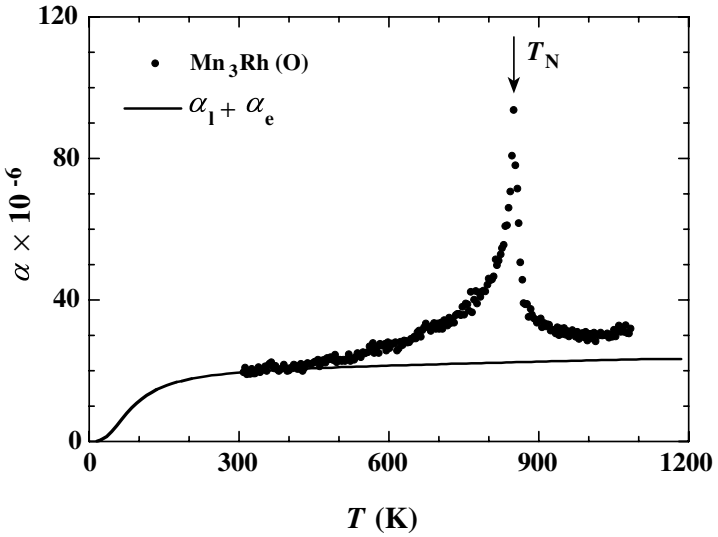

Figure 6. Temperature dependence of the thermal expansion coefficient α of the Mn_3Rh ordered (O) alloy. The solid curve stands for the sum of the lattice and the electronic contributions ($\alpha_l + \alpha_e$).

Table 1. The calculated total energy (ΔE in mRyd/atom), the magnetic moment (M in μ_B), the effective exchange constant (J_0 in millielectronvolts), the Néel temperatures (T_N^{cal} in kelvin) estimated from $2J_0/3k_B$, the Néel temperatures (T_N^{exp} in kelvin) obtained by the experiments and the electronic specific heat coefficient obtained by the calculation (γ^{cal} in mJ mol^{-1} K^{-2}) and experiment (γ^{exp} in mJ mol^{-1} K^{-2}) for the Mn_3Rh ordered (O) and disordered (DO) alloys.

Phase	Spin	ΔE	M_{Mn}	M_{Rh}	J_0	T_N^{cal}	T_N^{exp}	γ^{cal}	γ^{exp}
Ordered (O)	T1	0	2.78	0.00	163	1250	855	∼1.6	4.0
Disordered (DO)	3Q	7.3	2.66	0.08	88	680	∼700	∼2.2	4.6

be deduced from $2J_0/3k_B$ [42]. The calculated T_N for the ordered alloy is higher than that of the disordered one in accordance with the experimental data [8, 12]. The values of γ^{cal} are qualitatively consistent with the values of γ^{exp}, though the former values are smaller than the latter values. In addition, the point to observe is that the experimental γ^{exp}-values of the $Mn_{3.20}Rh_{0.80}$ are about twice as large as those of the Mn_3Rh in the ordered and disordered states as shown in figure 3. This would come from the change in the electronic structure because of the off-stoichiometric composition of Mn_3Rh.

The dotted curve in figure 6 represents the temperature dependence of the thermal expansion coefficient α of the Mn_3Rh ordered (O) alloy. A large positive peak is observed at the Néel temperature T_N. It should be emphasized that α above T_N shows a large value of about 30×10^{-6} K^{-1}. The volume thermal expansion coefficient $\omega = 3\alpha$ and specific heat C are related with the following Grüneisen relation [43]:

$$\alpha = \frac{1}{3}\omega = \frac{1}{3}\frac{\Gamma\kappa C}{V}, \tag{2}$$

where Γ is the Grüneisen parameter, κ the compressibility and V the molar volume. In general, the total thermal expansion coefficient is expressed as the sum of the lattice, electronic and magnetic contributions. In the present study, the sum of the lattice and electronic contributions

to the thermal expansion coefficient is defined as

$$\alpha_l + \alpha_e = \frac{1}{3}\frac{\Gamma\kappa(C_l + C_e)}{V} \tag{3}$$

with

$$C_l = 9Nk_B\left(\frac{T}{\Theta_D}\right)^3 \int_0^{\Theta_D/T} \mathrm{d}x \frac{x^4 \mathrm{e}^x}{(\mathrm{e}^x - 1)^2} \tag{4}$$

and

$$C_e = \gamma T, \tag{5}$$

where C_l and C_e stand for the lattice and the electronic contributions to the specific heat, respectively. N, k_B and γ are the number of atoms, the Boltzmann constant and the electronic specific heat coefficient, respectively. The lattice contribution $C_l(\alpha_l)$ can be described by the Debye theory, independent of temperature above the Debye temperature Θ_D. The electronic contribution $C_e(\alpha_e)$ is proportional to temperature. The solid curve in the figure stands for the sum of contributions of α_l and α_e to the thermal expansion coefficient calculated by equations (3)–(5). In the present calculations, the proportional coefficient Γ-value is defined as to meet the calculated value $(\alpha_l + \alpha_e)$ with the observed curve around room temperature and becomes an appropriate value of about 1.4 [44], using the κ-value given in figure 12. The observed α in paramagnetic regions is about 30×10^{-6} K^{-1}, much larger than the calculated value $(\alpha_l + \alpha_e)$ given by the solid curve in figure 6. It is difficult to explain such a large α of the Mn_3Rh ordered alloy as the sum of the lattice and the electronic contributions. According to the spin fluctuation theory, the thermal expansion coefficient is related to the temperature dependence of the spontaneous volume magnetostriction ω_s, expressed by [45, 46]

$$\omega_s = \kappa C_c(M^2 + \xi^2), \tag{6}$$

where κ, C_c, M and ξ are the compressibility, the coupling constant, the magnetization and the amplitude of local thermal spin fluctuations, respectively. In the paramagnetic state, M is zero; on the other hand, ξ shows an effective value. Therefore, the thermal expansion coefficient increases with the temperature in the paramagnetic state for itinerant-electron materials. We may recall that the strong spin fluctuation effect persists up to the temperature of about $3T_N$ for the YMn_2 compound, which exhibits a remarkably large α of about 55×10^{-6} K^{-1} above T_N [47].

Figure 7 shows the thermal expansion curves of the $Mn_{3+x}Rh_{1-x}$ ($x = 0.0$, 0.12 and 0.20) ordered (O) alloys, together with that of $Mn_{3.28}Pt_{0.72}$ [7] and Mn_3Ir [9] ordered (O) alloys. In the figure, the arrows indicate the Néel temperature T_N. The value of ΔL is defined as the difference between the room temperature length L_0 and the length at T, L. The broken arrows for the $Mn_{3.12}Rh_{0.88}$ alloy indicate the heating and the cooling processes. These data completely coincide with each other, proving that the magnetic transition is of the second order. The values of the thermal expansion coefficient α in the paramagnetic region for the $Mn_{3.28}Pt_{0.72}$ and Mn_3Ir ordered alloys are about 40 and 30×10^{-6} K^{-1}, respectively. Such a large thermal expansion coefficient in paramagnetic regions for γ-phase Mn alloys is evidence that these alloys have an itinerant-electron character with significant spin fluctuations as discussed in connection with figure 6. In addition, $Y_6(Mn_{1-x}Fe_x)_{23}$ [48], β-MnOs [49] and β-MnIr [50] alloys show a relatively large value of about 30×10^{-6} K^{-1}. For the $Mn_{3+x}Rh_{1-x}$ ordered alloys as well as the $Mn_{3.28}Pt_{0.72}$ [7] and Mn_3Ir [9] ordered alloys having the T1-type spin structure shown in figure 4(a), a negative magnetovolume effect is observed in their thermal expansion curves below T_N as seen from the figure. The thermal expansion curves of $Mn_{3.12}Rh_{0.88}$ and $Mn_{3.20}Rh_{0.80}$ disordered (DO) alloys are shown in figure 8, in which L_0 is the length of the specimen at room temperature. Although the anomaly at T_N indicated by the arrows is not

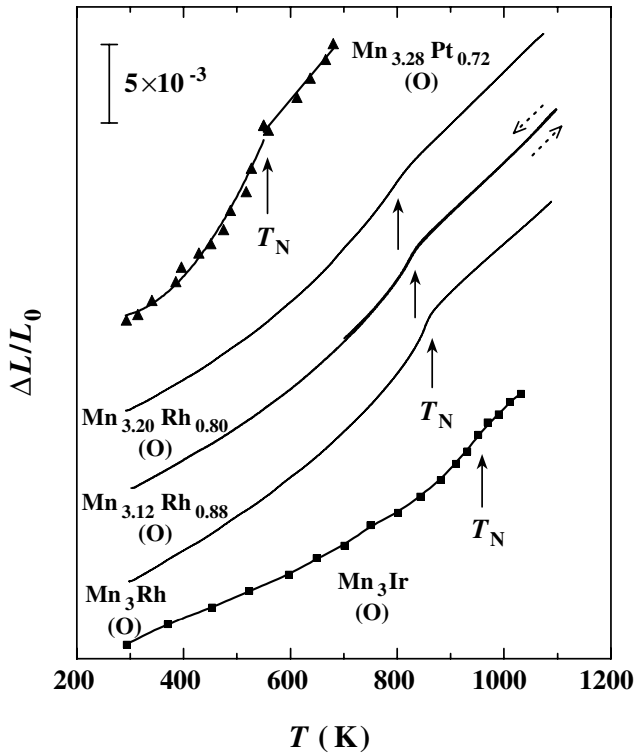

Figure 7. Thermal expansion curves of the $Mn_{3+x}Rh_{1-x}$ ordered (O) alloys, together with that of the $Mn_{3.28}Pt_{0.72}$ [7] and Mn_3Ir [9] ordered (O) alloys. The Néel temperature T_N is given by the arrows.

so clear, it can be said that a negative magnetovolume effect is also observed below T_N in analogy with the ordered alloys (see figure 7). An additional anomaly observed around 900 K in both the alloys is caused by the atomic ordering in a similar manner as the temperature dependence of electrical resistivity given in figure 2. The thermal expansion coefficient in paramagnetic regions above T_N to around 900 K is about 30×10^{-6} K^{-1}, much larger than that of 3d nonmagnetic elements [51]. As mentioned above, the anomaly at T_N is observed more clearly in the thermal expansion curve for the ordered alloy. This is in conformity with the fact that the calculated magnetic moment M_{Mn} of Mn atom for the ordered alloy is about 4% larger than that of the disordered one as listed in table 1, because the magnitude of the magnetic moment correlates to the magnitude of the spontaneous volume magnetostriction as expressed by equation (6).

Figure 9 shows the temperature dependence of electrical resistivity under various pressures for the Mn_3Rh ordered (O) alloy. Because the measurements were made by a quasi-four-probe method using a multianvil-type system, the background noises are somewhat high compared with the data in figure 1. Thus, the measurements were carried out twice to confirm the reproducibility. A clear change in electrical resistivity at T_N is confirmed as given by the fine solid lines as guides to the eyes. The Néel temperature T_N indicated by the arrows increases on applying pressure. In figure 6, a definite positive peak in the thermal expansion coefficient curve is observed at T_N. In other words, the $Mn_{3+x}Rh_{1-x}$ ordered alloy system has a negative magnetovolume effect below T_N. It is well known that the magnetovolume effect

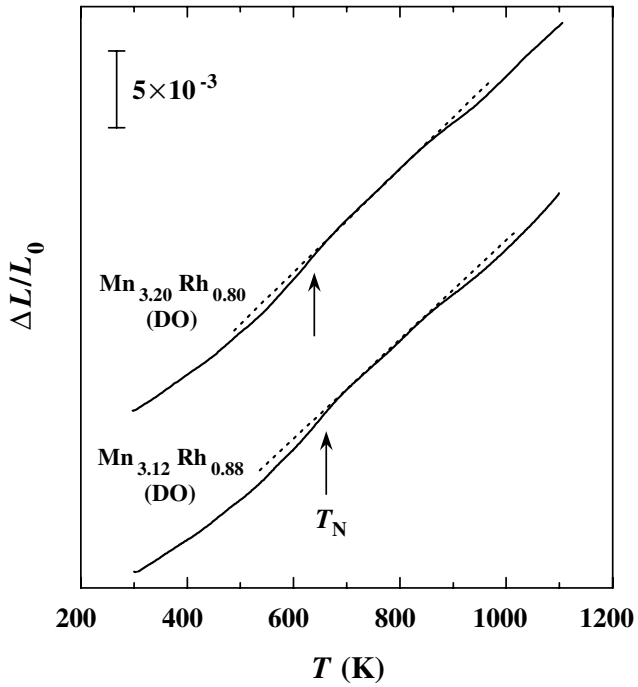

Figure 8. Thermal expansion curves of the $Mn_{3.12}Rh_{0.88}$ and $Mn_{3.20}Rh_{0.80}$ disordered (DO) alloys. The Néel temperature T_N is given by the arrows. The broken lines are guides to the eyes.

is thermodynamically correlated to the pressure dependence of T_N. The Ehrenfest expression for the second-order transformation is given by

$$\frac{dT_N}{dP} = VT_N\frac{\Delta\alpha_V}{\Delta C}, \tag{7}$$

where P and V are pressure and volume, respectively. The differences between the values of thermal expansion coefficient and the specific heat below and above T_N are given by $\Delta\alpha_V$ and ΔC, respectively. The positive or the negative pressure dependence of T_N coincides with the sign of $\Delta\alpha_v$. To put it more concretely, the negative magnetovolume effect shown in figure 7 and the positive peak of the α curve in figure 6 should result in the increase in T_N by applying pressure. The pressure dependence of the Néel temperature T_N is given in figure 10. The closed circles and triangles indicate T_N of the Mn_3Rh and $Mn_{3.20}Rh_{0.80}$ ordered (O) alloys, respectively. The value of T_N for both the samples increases linearly in this pressure region, and the value of dT_N/dP is estimated to be about 7.0–8.0 K GPa^{-1}.

Presented in figure 11 are the room temperature x-ray powder diffraction patterns by an energy-dispersive mode under various pressures for the Mn_3Rh ordered (O) alloy. The measurements were made in the condition of a fixed diffraction angle and the applied pressures were calibrated by Decker's scale using the lattice constant of a reference sample of NaCl [52]. In the figure, the observed peaks can be indexed as an $AuCu_3$-type structure, though there are peaks from the boron nitride (BN) disc used to separate the powdered sample and NaCl, and the characteristic spectra of Rh Kα and Kβ. The peaks of the sample shift to higher energy on applying pressure, and the pressure dependence of the volume V of the Mn_3Rh ordered (O) alloy is drawn in figure 12. The value of ΔV is defined as the difference between the volumes under the ambient and the applied pressures, V_0 and V, respectively. From the figure, the

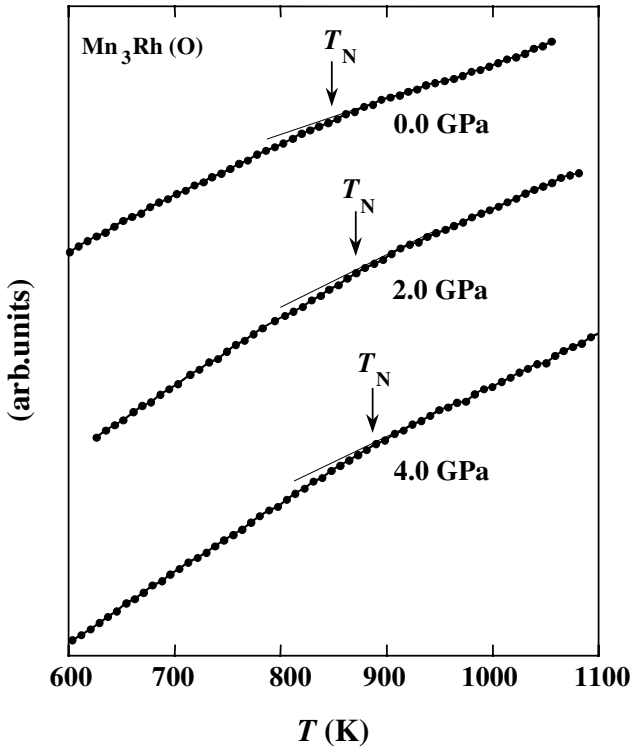

Figure 9. Temperature dependence of electrical resistivity ρ under various pressures for the Mn_3Rh ordered (O) alloy. The arrows indicate the Néel temperature T_N.

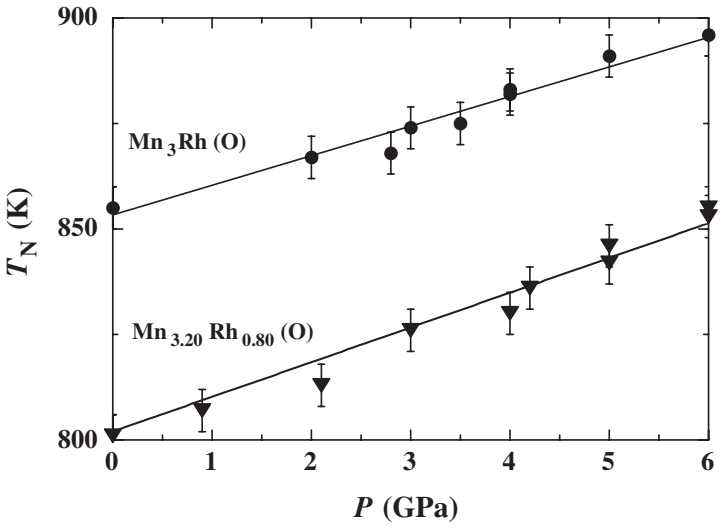

Figure 10. Pressure dependence of the Néel temperature T_N of the Mn_3Rh and $Mn_{3.20}Rh_{0.80}$ ordered (O) alloys.

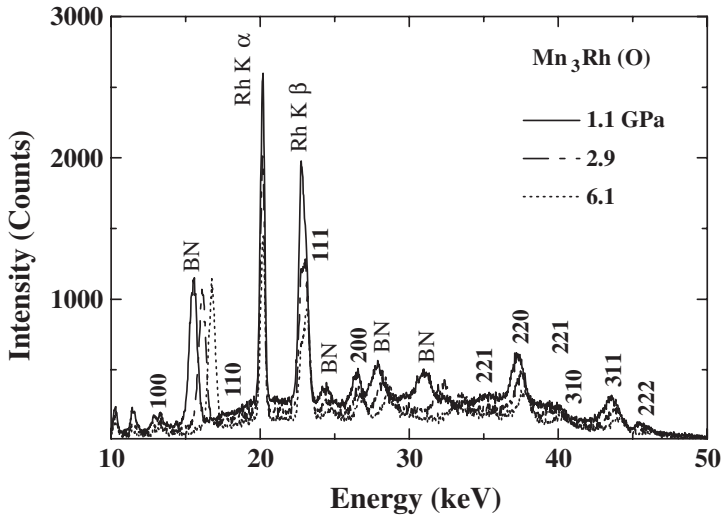

Figure 11. The room temperature x-ray powder diffraction patterns measured in an energy-dispersive mode at a fixed diffraction angle for the Mn_3Rh ordered (O) alloy under various pressures.

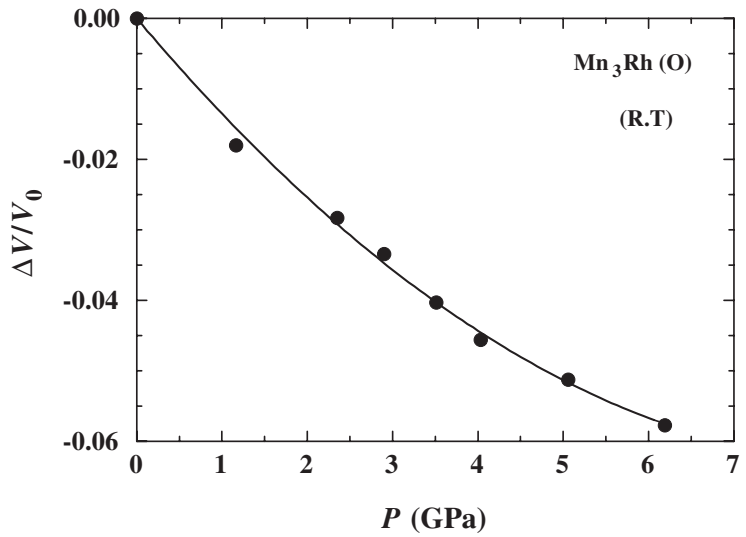

Figure 12. Pressure dependence of $\Delta V/V_0$ of the Mn_3Rh ordered (O) alloy. The value of ΔV indicates the difference between the volume under ambient pressure V_0 and the volume under applied pressure V at room temperature (RT).

compressibility κ is deduced as the coefficient of the first term by fitting to the second-order function of the pressure P given by

$$\Delta V/V_0 = aP + bP^2. \tag{8}$$

The compressibility $\kappa = -\mathrm{d}\ln V/\mathrm{d}\ln P$ of the Mn_3Rh ordered alloy is estimated to be about 1.4×10^{-2} GPa^{-1}, more compressible than that of an α-Mn of about 0.8×10^{-2} GPa^{-1} at room temperature [21]. The Néel temperature T_N of α-Mn is 95 K [53]; the difference

in compressibility between the paramagnetic and the antiferromagnetic states is as small as 6% [54]. The reason for such a small difference has been attributed to the existence of the localized magnetic moments in the paramagnetic state [53, 55].

It is well known that the bulk modulus is generally lowered by the appearance of magnetism, especially in antiferromagnets [22, 23, 56]. It has been reported that the bulk modulus of the magnetic elements in 3d transition metals is deviant from the experimental results in the early theoretical calculations by the local-density approximation (LDA) [22, 23]. However, the lattice constant and the magnetic moments of Mn calculated by the generalized gradient approximation (GGA) [57] are nearly in agreement with the experimental results [58, 59]. From the GGA, the bulk modulus and the magnetic moments of the fcc-Mn, that is, γ-Mn in the antiferromagnetic phase, are 1.07×10^2 GPa, corresponding to 0.93×10^{-2} GPa^{-1} in κ, and 2.13 μ_B, respectively, and the values of the bcc-Mn in the antiferromagnetic phase are 0.77×10^2 GPa, corresponding to 1.30×10^{-2} GPa^{-1} in κ, and 2.73 μ_B, respectively. The value of γ-Mn is close to the present experimental result for the Mn_3Rh ordered alloy. Although no calculated results for α-Mn are available, it should be pointed out that there is a close relationship between the compressibility and the magnitude of the localized magnetic moment in 3d transition metals and alloys [24], and the large value of κ for α-Mn would be considered to result from the existence of localized magnetic moment. There are four inequivalent atomic sites in α-Mn and their magnetic moments at sites I, II, III and IV have been reported to be 1.9, 1.7, 0.6 and 0.2 μ_B in the ground state, respectively [14]. However, it should be pointed out that the number of Mn atoms at the sites I and II with the large magnetic moments that are close to 2 μ_B is less than 20% in the whole unit cell. That is, most of the Mn atoms of α-Mn carry a small magnetic moment. We may notice that the magnetic moment for the γ-phase Mn alloys is much larger than that for α-Mn (see table 1). On the other hand, it has been pointed out that a systematic change in bonding mechanism in antiferromagnetic materials contributes to lowering the modulus [56]. Furthermore, it is important to keep in mind that many experimental values have been obtained at room temperature, whereas the theoretical values are in the ground state. In equation (6), the spin fluctuation term for ξ^2 is convex downward at low temperatures and exhibits a linear increase at high temperatures [46], and hence both the lattice vibrations and the spin fluctuations would bring about the increase in κ at finite temperature. It calls for further investigations from the theoretical and experimental view points in order to come to clear explanations for the large values of κ of the γ-phase MnRh and α-Mn.

For the additives Ir and Rh, belonging to the same group in the periodic table, the lattice constant of the Mn_3Ir ordered alloy is smaller than that of the Mn_3Rh ordered alloy. The room temperature lattice constant of the Mn_3Ir ordered alloy is comparable with the value of the Mn_3Rh ordered alloy under applied pressure of about 2.0 GPa [13]. On the other hand, the Néel temperature of 960 K for the Mn_3Ir ordered alloy is much higher than the value of 855 K for the Mn_3Rh ordered alloy [9, 11]. However, figure 10 indicates that T_N of the latter does not go up to T_N of the former under the corresponding pressure of 2.0 GPa. Therefore, the strength of the exchange interaction of Mn systems cannot be explained by the Mn–Mn distance, or the localized magnetic moment model.

Finally, we would like to give important comments from practical viewpoints. In fabrication processes of spin-valve devices composed of multilayers, the substrate temperature would rise above room temperature. In such circumstances, it is expected that thermal strains [60] are inevitably induced in these multilayers due to the difference in the thermal expansion coefficient between the film layers and also the substrate. Recently, it has been demonstrated that the Néel temperature of $LaFeO_3$ film is significantly changed by strains relative to the bulk material [61]. Compared with the bulk specimens, the γ-phase Mn alloy

film layer would be liable to induce a marked change in the Néel temperature because of the large thermal expansion coefficient and the high compressibility, reflected in the exchange biasing characteristics and the blocking temperature. Practically, the magnetovolume effects and the thermal strains cannot be ignored because they are closely correlated with durability and stability of spin-valves. In other words, these strains would easily accelerate diffusions associated with electromigration and stress migration, causing deterioration of the spin-valve characteristics. For antiferromagnetic materials used as spin-valve devices, γ-phase MnIr disordered alloys have been most intensively investigated [25–27]. In figure 7, the thermal expansion properties of the Mn_3Ir ordered alloy are similar to those of Mn_3Rh, which show a negative magnetovolume effect and a large thermal expansion coefficient in paramagnetic regions. Accordingly, we can expect that the thermal expansion characteristics of γ-phase MnIr disordered alloys are similar to those of the γ-phase MnRh disordered alloys given in figure 8.

4. Conclusion

The electrical resistivity, low-temperature specific heat, thermal expansion, pressure effects on the Néel temperature and compressibility of the $Mn_{3+x}Rh_{1-x}$ ordered and disordered alloys have been investigated. In addition, the total energies of the magnetic structures of the Mn_3Rh ordered and disordered alloys have been discussed. It is clarified that the large thermal expansion coefficient observed in the paramagnetic state is characterized by the effect of spin fluctuations. The behaviour of the pressure dependence of the Néel temperature is consistent with the negative magnetovolume effect. The results from the theoretical calculations of the electronic structures implying a stable antiferromagnetic order are in accordance with the experimental data. The main results are summarized as follows.

(a) The electrical resistivity of the $Mn_{3+x}Rh_{1-x}$ ordered and disordered alloys exhibits a characteristic behaviour of gapless-type antiferromagnets, accompanied by a steeper decrease below the Néel temperature.

(b) A negative magnetovolume effect is observed in the $Mn_{3+x}Rh_{1-x}$ ordered and disordered alloys. The thermal expansion coefficient in the paramagnetic region shows a very large value of about 30×10^{-6} K^{-1}. This behaviour is caused by a large magnetic contribution from spin fluctuations.

(c) The experimental electronic specific heat coefficient γ^{exp} of the ordered alloys is smaller than that of the disordered alloys, qualitatively consistent with the theoretical calculations. The dip formed around the Fermi level in the electronic structures is more distinct in the ordered phase.

(d) For the Mn_3Rh alloys, the calculated magnetic moment of the T1-type spin structure in the ordered phase is larger than that of a $3Q$ structure in the disordered phase.

(e) The Néel temperature T_N increases with the applied pressure, consistent with the negative magnetovolume effect. The pressure shift of the Néel temperature, $\mathrm{d}T_N/\mathrm{d}P$, is 7.0–8.0 K GPa^{-1} for the Mn_3Rh and $Mn_{3.20}Rh_{0.80}$ ordered alloys.

(f) The compressibility of the Mn_3Rh ordered alloy is estimated to be about 1.4×10^{-2} GPa^{-1}, much larger than that of α-Mn.

(g) Between Mn_3Rh and Mn_3Ir ordered alloys, the comparisons of the lattice constant and the Néel temperature T_N imply that the strength of the exchange interaction of Mn systems cannot be explained by the Mn–Mn distance, or the localized magnetic moment model.

Acknowledgments

One of the authors (R Y Umetsu) has been supported by the Research Fellowships of the Japanese Society for the Promotion of Science for Young Scientists. The present work has been supported by a Grant-in-Aid for Scientific Research (B)(2), No 13450225, from the Japanese Society for the Promotion of Science.

References

[1] Young D A 1991 *Phase Diagrams of the Elements* (Berkeley, CA: University of California Press) p 2595
[2] Bacon G E, Dunmur I W, Smith J H and Street R 1957 *Proc. R. Soc.* A **241** 223
[3] Endoh Y, Ishikawa Y and Shinjo T 1969 *Phys. Lett.* A **29** 310
[4] Hicks T J, Pepper A R and Smith J H 1968 *J. Phys. C: Solid State Phys.* **1** 1683
[5] Uchishiba H, Hori T and Nakagawa Y 1970 *J. Phys. Soc. Japan* **28** 792
[6] Raub R and Mahler W 1955 *Z. Metallkd.* **46** 282
[7] Krén E, Kádár G, Pál L, Szabó P and Tarmóczi T 1968 *Phys. Rev.* **171** 574
[8] Krén E, Kádár G, Pál L, Sólyom J and Szabó P 1966 *Phys. Lett.* **1** 331
[9] Tomeno I, Fuke H N, Iwasaki H, Sahashi M and Tsunoda Y 1999 *J. Appl. Phys.* **86** 3853
[10] Krén E 1966 *Phys. Lett.* **21** 383
[11] Yamaoka T 1974 *J. Phys. Soc. Japan* **36** 445
[12] Yamauchi R, Fukamichi K, Yamauchi H, Sakuma A and Echigoya J 1999 *J. Appl. Phys.* **85** 4741
[13] Yamaoka T, Mekata M and Takaki H 1974 *J. Phys. Soc. Japan* **36** 438
[14] Yamada T, Kunitomi N, Nakai Y, Cox D E and Shirane G 1970 *J. Phys. Soc. Japan* **28** 615
[15] Krén E, Kádár G, Pál L and Szabó P 1967 *J. Appl. Phys.* **38** 1265
[16] Yasui H, Kaneko T, Yoshida H, Abe S, Kamiguchi K and Môri N 1987 *J. Phys. Soc. Japan* **56** 4532
[17] Shirai M, Tanimoto T and Motizuki K 1990 *J. Magn. Magn. Mater.* **90/91** 157
[18] Yamauchi R, Fukamichi K, Yamauchi H and Sakuma A 1998 *J. Alloys Compounds* **279** 93
[19] Yamauchi R, Hori T, Miyakawa M and Fukamichi K 2000 *J. Alloys Compounds* **309** 16
[20] Sakuma A 1999 *IEEE Trans. Magn.* **35** 3349
[21] Takemura K, Shimomura O, Hase K and Kikegawa T 1988 *J. Phys. F: Met. Phys.* **18** 197
[22] Janak J F and Williams A R 1976 *Phys. Rev.* B **14** 4199
[23] Moruzzi V L, Williams A R and Janak J F 1977 *Phys. Rev.* **15** 2854
[24] Môri N, Takahashi M and Oomi G 1983 *J. Magn. Magn. Mater.* **31–34** 135
[25] Fuke H N, Saito K, Yoshikawa M, Iwasaki H and Sahashi M 1999 *Appl. Phys. Lett.* **75** 3680
[26] Devasahayam A J, Sides P J and Kryder M H 1998 *J. Appl. Phys.* **83** 7216
[27] Wang D, Tondra M, Nordman C and Daughton J M 1999 *IEEE Trans. Magn.* **35** 2886
[28] Veloso A, Freitas P P, Oliveira N J, Fernandes J and Ferreira M 1998 *IEEE Trans. Magn.* **34** 2343
[29] Sun J J and Freitas P P 1999 *J. Appl. Phys.* **85** 5264
[30] Malozemoff A P 1987 *Phys. Rev.* B **35** 3679
[31] Koon N C 1997 *Phys. Rev. Lett.* **78** 4865
[32] Schulthess T C and Butler W H 1999 *J. Appl. Phys.* **85** 5510
[33] Sakuma A, Fukamichi K, Sasao K and Umetsu R Y 2003 *Phys. Rev.* B **67** 024420 1-7
[34] Sakuma A, Umetsu R Y and Fukamichi K 2002 *Phys. Rev.* B **66** 014432 1-6
[35] Sakuma A 2000 *J. Phys. Soc. Japan* **69** 3072
[36] Suezaki Y and Mori H 1969 *Prog. Theor. Phys.* **41** 1177
[37] Rossiter P L 1980 *J. Phys. F: Met. Phys.* **10** 1459
[38] Umetsu R Y, Fukamichi K and Sakuma A 2002 *J. Appl. Phys.* **91** 8873
[39] Umetsu R Y, Fukamichi K and Sakuma A 2002 *J. Magn. Magn. Mater.* **239** 530
[40] Honda N, Tanji Y and Nakagawa Y 1976 *J. Phys. Soc. Japan* **41** 1931
[41] Hori T, Morii Y, Funahashi S, Niida H, Akimitsu M and Nakagawa Y 1995 *Physica* B **213/214** 354
[42] Liechtenstein A I, Katsnelson M I, Antropov V P and Gubanov V A 1987 *J. Magn. Magn. Mater.* **67** 65
[43] Gopal E S R 1966 *Specific Heats at Low Temperatures* (New York: Plenum)
[44] Barron T H K, Collins J G and White G K 1980 *Adv. Phys.* **29** 609
[45] Moriya T and Usami K 1980 *Solid State Commun.* **34** 95
[46] Yamada H 1995 *J. Magn. Magn. Mater.* **139** 162
[47] Shiga M, Wada H, Nakamura H, Yoshimura K and Nakamura Y 1987 *J. Phys. F: Met. Phys.* **17** 1781
[48] Ohta M, Fujita A, Fukamichi K, Matsubara E and Takahashi H 2002 *J. Phys.: Condens. Matter* **14** 5785

[49] Miyakawa M, Umetsu R Y and Fukamichi K 2001 *J. Phys.: Condens. Matter* **13** 3809
[50] Miyakawa M, Umetsu R Y, Sasao K and Fukamichi K 2003 *J. Phys.: Condens. Matter* to be submitted
[51] Carr W J Jr 1979 *J. Magn. Magn. Mater.* **10** 197
[52] Decker D L 1971 *J. Appl. Phys.* **42** 3239
[53] Shull C G and Wilkinson M K 1953 *Rev. Mod. Phys.* **25** 100
[54] Rosen M 1968 *Phys. Rev.* **165** 357
[55] Kasper J S and Roberts B W 1956 *Phys. Rev.* **101** 537
[56] Sliwko V, Mohn P and Schwarz K 1994 *J. Phys.: Condens. Matter* **6** 6557
[57] Perdew J P and Wang Yue 1986 *Phys. Rev.* B **33** 8800
[58] Asada T and Terakura K 1993 *Phys. Rev.* B **47** 15992
[59] Asada T and Terakura K 1992 *Phys. Rev.* B **46** 13599
[60] Koike J, Utsunomiya S, Shimoyama Y, Maruyama K and Oikawa H 1998 *J. Mater. Res.* **13** 3256
[61] Scholl A, Stöhr J, Lüning J, Seo J W, Fompeyrine J, Siegwart H, Locquet J-P, Nolting F, Anders S, Fullerton E E, Scheinfein M R and Padmore H A 2000 *Science* **287** 1014